A therapeutic T cell receptor mimic antibody targets tumor-associated PRAME peptide/HLA-I antigens

Aaron Y. Chang, … , Cheng Liu, David A. Scheinberg

Research Article Immunology Therapeutics

Preferentially expressed antigen in melanoma (PRAME) is a cancer-testis antigen that is expressed in many cancers and leukemias. In healthy tissue, PRAME expression is limited to the testes and ovaries, making it a highly attractive cancer target. PRAME is an intracellular protein that cannot currently be drugged. After proteasomal processing, the PRAME[300–309] peptide ALYVDSLFFL (ALY) is presented in the context of human leukocyte antigen HLA-A*02:01 molecules for recognition by the T cell receptor (TCR) of cytotoxic T cells. Here, we have described Pr20, a TCR mimic (TCRm) human IgG1 antibody that recognizes the cell-surface ALY peptide/HLA-A2 complex. Pr20 is an immunological tool and potential therapeutic agent. Pr20 bound to PRAME[+]HLA-A2[+] cancers. An afucosylated Fc form (Pr20M) directed antibody-dependent cellular cytotoxicity against PRAME[+]HLA-A2^{+} leukemia cells and was therapeutically effective against mouse xenograft models of human leukemia. In some tumors, Pr20 binding markedly increased upon IFN-γ treatment, mediated by induction of the immunoproteasome catalytic subunit β5i. The immunoproteasome reduced internal destructive cleavages within the ALY epitope compared with the constitutive proteasome. The data provide rationale for developing TCRm antibodies as therapeutic agents for cancer, offer mechanistic insight on proteasomal regulation of tumor-associated […]

Find the latest version:

https://jci.me/92335/pdf

A therapeutic T cell receptor mimic antibody targets tumor-associated PRAME peptide/HLA-I antigens

Aaron Y. Chang,[1,2] Tao Dao,[1] Ron S. Gejman,[1,3] Casey A. Jarvis,[1] Andrew Scott,[1,4] Leonid Dubrovsky,[1] Melissa D. Mathias,[1] Tatyana Korontsvit,[1] Victoriya Zakhaleva,[1] Michael Curcio,[1] Ronald C. Hendrickson,[1] Cheng Liu,[5] and David A. Scheinberg[1,3]

[1]Molecular Pharmacology Program, Memorial Sloan Kettering Cancer Center (MSKCC), New York, New York, USA. [2]Biochemistry Cell and Molecular Biology Program, [3]Pharmacology Program, and [4]Immunology and Microbial Pathogenesis Program, Weill Cornell Medicine, Cornell University, New York, New York, USA. [5]Eureka Therapeutics, Emeryville, California, USA.

Preferentially expressed antigen in melanoma (PRAME) is a cancer-testis antigen that is expressed in many cancers and leukemias. In healthy tissue, PRAME expression is limited to the testes and ovaries, making it a highly attractive cancer target. PRAME is an intracellular protein that cannot currently be drugged. After proteasomal processing, the PRAME[300–309] peptide ALYVDSLFFL (ALY) is presented in the context of human leukocyte antigen HLA-A*02:01 molecules for recognition by the T cell receptor (TCR) of cytotoxic T cells. Here, we have described Pr20, a TCR mimic (TCRm) human IgG1 antibody that recognizes the cell-surface ALY peptide/HLA-A2 complex. Pr20 is an immunological tool and potential therapeutic agent. Pr20 bound to PRAME+HLA-A2+ cancers. An afucosylated Fc form (Pr20M) directed antibody-dependent cellular cytotoxicity against PRAME+HLA-A2+ leukemia cells and was therapeutically effective against mouse xenograft models of human leukemia. In some tumors, Pr20 binding markedly increased upon IFN-γ treatment, mediated by induction of the immunoproteasome catalytic subunit β5i. The immunoproteasome reduced internal destructive cleavages within the ALY epitope compared with the constitutive proteasome. The data provide rationale for developing TCRm antibodies as therapeutic agents for cancer, offer mechanistic insight on proteasomal regulation of tumor-associated peptide/HLA antigen complexes, and yield possible therapeutic solutions to target antigens with ultra-low surface presentation.

Introduction

Effective and safe cancer therapy is premised on the idea that neoplastic cells can be specifically identified and eliminated while healthy cells remain unharmed. Although a large number of cancer-specific changes in the cell have been identified, including tumor-specific mutations, glycosylation patterns, and gene expression signatures, the vast majority of these cancer-specific markers and tumor-associated antigens cannot currently be targeted with either small molecule inhibitors or traditional Abs. Recently, a strategy to target these heretofore-untargetable epitopes has been developed by use of T cell receptor (TCR) mimic mAbs (TCRm). TCRm have specificities similar to those of T cell receptors and are directed to peptides presented in complex with MHC or HLA-I. In contrast with TCR-based therapies, TCRm can be delivered to patients as off-the-shelf pharmaceutical agents in a variety of formats ranging from IgG to bispecific T cell engagers (BiTEs), which allows for exquisite control over handling and pharmacology. In the pres-

ent study, we designed a TCRm against the cancer-testis antigen preferentially expressed antigen in melanoma (PRAME) and studied the regulation of the epitope expression.

Cancer-testis antigens are a group of tumor antigens that are overexpressed in many cancers, but exhibit limited expression in healthy adult tissue except for in the testes, ovaries, and endometrium (1). The protein PRAME is a cancer-testis antigen that is overexpressed in a broad range of cancer types, including primary and metastatic melanoma (80%–90% of cases) (1, 2), breast cancer (27% of cases) (3), and neuroblastoma (>90% of cases) (3, 4). PRAME is also highly expressed in hematopoietic malignancies including acute myeloid leukemia (AML) (40%–60% of cases) (5, 6), acute lymphoblastic leukemia (ALL) (20%–40% of cases) (1, 6), myeloma (20%–50% of cases) (1), and chronic myeloid leukemia (CML) (30%–40% of cases) (1, 7). PRAME expression has been linked to poor prognosis in breast cancer (8) and neuroblastoma (4). PRAME is also expressed in the stem cells of CML (9), suggesting that targeting PRAME could preferentially deplete the leukemia-initiating cell population. PRAME is a retinoic acid receptor–binding protein that functions to block retinoic acid–mediated proliferation arrest, differentiation, and apoptosis (1, 10). This tumor-selective expression profile makes PRAME a highly attractive therapeutic target.

PRAME is an intracellular protein (1, 11, 12), making it impossible to target using traditional Abs directed at cell-surface proteins, and it cannot currently be inhibited using small molecules. Its function in tumor progression is complex, and in some contexts, PRAME overexpression can reduce malignancy

of leukemia in vivo (11). Due to its context-dependent role of both promoting and inhibiting tumorigenesis, direct functional inhibition of the protein may not prove to be therapeutically effective as compared to cytotoxicity against PRAME-expressing cells. After proteasomal processing, PRAME-derived peptides, including the PRAME[300–309] peptide ALYVDSLFFL (ALY), are presented on the cell surface in the context of HLA-A*02:01 (HLA-A2) molecules (13, 14). HLA-A2 is the most common HLA-I subtype, found in approximately 40% of the United States population (15), and generating cancer immunotherapies against antigens presented by HLA-A2 would benefit a substantial population. Several groups have demonstrated the ability to generate ALY/HLA-A2–specific CD8 cytotoxic T lymphocytes (CTLs) that can specifically lyse PRAME+HLA-A2+ tumors and are reactive against primary leukemia (16–18), providing proof that this epitope is presented and can be targeted by immunotherapy. Clinical trials have also demonstrated that patients vaccinated against PRAME can develop PRAME-specific CTLs (19) and helper T cells (20). There are several major constraints to cellular and vaccine-based strategies. CTL-based therapies are patient specific and often require laborious manipulation before reinfusion, while vaccines may be less potent and responses are difficult to predict or control, depending on the patient's immune repertoire and immunological status (21).

mAbs have demonstrated potent antitumor efficacy in the clinic. Despite promising results, a major limitation of currently marketed mAbs is that they bind exclusively to cell-surface and extracellular antigens, whereas the majority of aberrantly expressed proteins in cancer, including PRAME, are intracellular (1, 11, 12, 15). We hypothesized that a TCRm Ab directed against the peptide-HLA complex formed by ALY and HLA-A2 would be capable of specifically binding to PRAME-expressing tumors and would be a cancer therapeutic against a formerly untargetable protein.

Presentation of tumor-associated antigens requires appropriate protein degradation, typically through the proteasome, additional processing steps, and loading onto HLA-I in the endoplasmic reticulum. Peptides presented by HLA-A2 are typically 9–11 residues in length and require hydrophobic anchor residues at the second and last position (22). The proteasome is a multisubunit complex that can exist in 2 major forms: the constitutive proteasome and the immunoproteasome, which have altered cleavage specificities and thus generate unique repertoires of peptides. They differ in 3 catalytic subunits: β1, β2, and β5 are found in the constitutive proteasome, while β1i, β2i, and β5i are part of the immunoproteasome (23–26). The immunoproteasome generally favors cleavage after hydrophobic residues, which enhances generation of peptides that can fit into the groove of HLA-I (23, 27). Several antigens are restricted to a specific proteasome form, and such knowledge can help dictate immunotherapy strategies against these targets (28).

We report the discovery and characterization of Pr20, which we believe is the first TCRm against PRAME, which we have generated to recognize the ALY peptide in complex with cell-surface HLA-A2. We characterized the ability of Pr20 to bind PRAME+ HLA-A2+ cancers and mediate cytotoxicity against PRAME-expressing malignancies in vitro and in vivo. In addition, we studied the role of the constitutive proteasome and immunoprotea-

some and their pharmacologic manipulation in generating the ALY peptide epitope, which may be important in the use of this and other TCR-based agents therapeutically.

Results

Pr20 binds to ALY/HLA-A2 complexes in PRAME/HLA-A2–expressing leukemias. TCRm clones reactive with ALY/HLA-A2 complexes were identified through a phage-display library screen as described previously (15). We aimed to identify a TCRm Ab that recognized ALY/HLA-A2, but not HLA-A2 alone or in complex with irrelevant HLA-A2–binding peptides. Briefly, single phage clones selective for the ALY/HLA-A2 complex were picked by a positive panning strategy on in vitro–folded ALY/HLA-A2 monomers and a negative panning strategy against RHAMM-R3/ HLA-A2 irrelevant peptide control monomers. Specificity of phage clones was further screened on live cells using transporter associated with antigen processing–deficient (TAP-deficient) HLA-A2+ T2 cells, (which have low levels of endogenously presented HLA-A2 peptides) pulsed with or without ALY or an irrelevant peptide. A more detailed description of phage-display library panning, positive clone screening, and single-chain variable fragment (scFv) characterization can be found in the Supplemental Methods (supplemental material available online with this article; https://doi.org/10.1172/JCI92335DS1). Four phage clones that selectively bound ALY peptide–pulsed T2 cells were engineered into full-length human IgG1. Pr20 IgG1 was selected as the lead clone after it was determined to have a low nM affinity (approximately 4–5 nM K_D), as measured by a binding assay with HLA-A2/ALY monomers using ForteBio and by Scatchard analysis of binding PRAME+HLA-A2+ AML14 cells (Supplemental Figure 1). mAb clones Pr8, Pr17, and Pr29 were not pursued due to nonspecific binding to HLA-A2+ healthy donor peripheral blood mononuclear cells (PBMCs), lower estimated affinity, or inability to bind to target cells, possibly due to subtle structural differences between in vitro–folded ALY/HLA-A2 and endogenously presented ALY/HLA-A2.

To determine the specificity of Pr20, T2 cells were pulsed with ALY peptide or with the irrelevant control EW peptide (Figure 1A). Pr20 did not bind T2 cells pulsed with the EW peptide, but readily bound T2 cells pulsed with the ALY peptide, as measured by flow cytometry, demonstrating that Pr20 bound to the ALY/HLA-A2 complex and not to HLA-A2 alone or an irrelevant peptide/HLA-A2 complex. To more carefully map the TCRm epitope, each residue on the ALY peptide was replaced with alanine (except the canonical anchor residues on positions 2 and 10, which are important for binding to HLA-A2) and Pr20 binding was assessed on peptide-pulsed T2 cells (Figure 1B). Single alanine residue substitutions on positions 5, 7, 8, and 9 reduced or abrogated Pr20 binding at a saturating concentration of Pr20, suggesting that Pr20 primarily contacted the ALY peptide's C-terminal half (Figure 1B). Decrease in Pr20 binding was not due to instability of peptide/HLA-A2 complexes, as each peptide increased surface HLA-A2 over unpulsed T2 cells in the assay, indicating that the peptides complexed with and stabilized HLA-A2 (Figure 1B). The data demonstrated that specific changes to the native peptide sequence can abrogate Pr20 binding, consistent with other reported TCRm (15, 29).
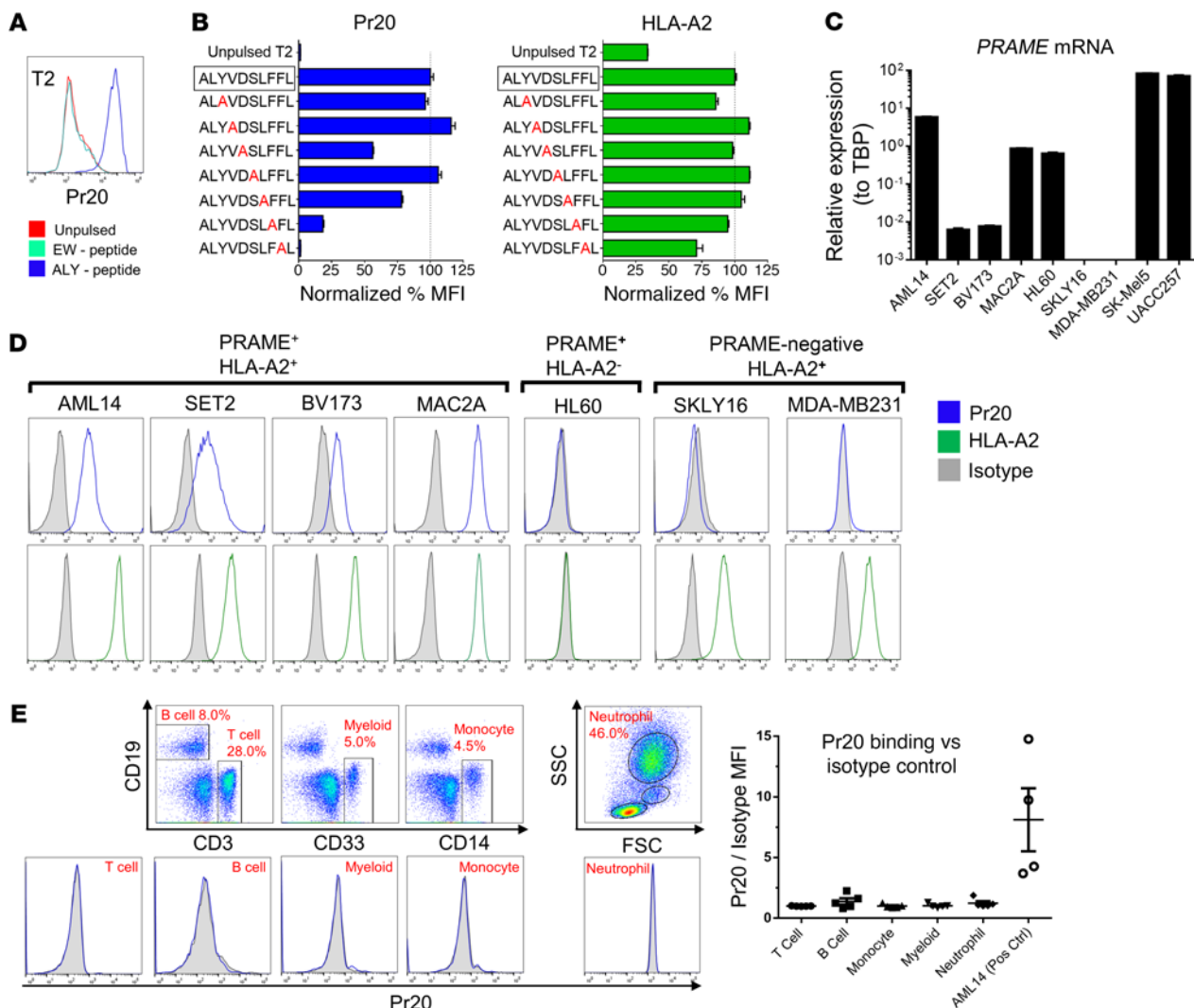
Figure 1. Pr20 binds ALY/HLA-A2 complexes and PRAME+HLA-A2+ leukemia. Pr20 was directly labeled by conjugation to the fluorophore APC. (**A**) TAP-deficient T2 cells were pulsed overnight with 50 μg/ml of ALY peptide or irrelevant control EW peptide or left unpulsed. Flow cytometry was used to determine P20 binding. (**B**) Each nonanchor residue in the ALY peptide was substituted for alanine, and peptides were pulsed onto T2. Pr20 binding was determined by flow cytometry relative to native ALY peptide–pulsed T2. Cell-surface HLA-A2 was also measured by flow cytometry to ensure altered peptides maintained the ability to bind and stabilize HLA-A2 compared with unpulsed T2. (**C**) *PRAME* mRNA expression was determined by qPCR, and samples that did not amplify after 40 cycles were considered negative. (**D**) The indicated cell lines were stained with Pr20 or an isotype control Ab, and binding was determined by flow cytometry. Surface HLA-A2 was also assessed compared with an isotype control. All data from **A**–**D** are representative of at least 3 experiments. (**E**) Whole blood populations from HLA-A2+ healthy donors were stained with Pr20 to determine possible crossreactivity. A representative gating strategy and Pr20 histogram compared with isotype control are shown, and data from all HLA-A2+ healthy donors (*n* = 5) are summarized. Staining was performed once independently for each healthy donor and an AML14 PRAME+HLA-A2+ leukemia–positive control was included in each assay to ensure assay reliability. SSC, side scatter; FSC, forward scatter.

After the preliminary biochemical and specificity characterization, we sought to determine whether Pr20 could recognize cancer cells expressing endogenous PRAME protein. *PRAME* mRNA expression was assessed by quantitative PCR (qPCR), and surface HLA-A2 expression and Pr20 binding were assessed by flow cytometry across a panel of HLA-A2+ hematopoietic and solid tumor cell lines, several of which have been reported to express PRAME by other groups (10, 12, 16, 30, 31) (Table 1 and Figure 1C). Pr20 binding was readily detected in PRAME+HLA-A2+ leukemia AML14, SET2, BV173, and the T cell lymphoma MAC2A, demonstrating that Pr20 can detectably bind endogenously processed and presented peptides (Figure 1D). Pr20 did not bind

the PRAME+HLA-A2− AML cell line HL60, indicating that the epitope was restricted by HLA-A2. In addition, Pr20 did not bind PRAME−HLA-A2+ tumors of various histological types, including SKLY16 lymphoma, MDA-MB231 breast adenocarcinoma, and NCI-H2228 lung carcinoma. (Figure 1D and Table 1). We detected minimal or no Pr20 binding on T, B, myeloid, monocyte, or neutrophil populations in whole blood taken from HLA-A2+ healthy donors (Figure 1E), demonstrating that Pr20 binds specifically to PRAME-positive tumors. To determine whether Pr20 bound primary human AML cells, we stained 9 frozen samples from HLA-A2+ AML patients and assayed for binding by flow cytometry. Only minimal positive shifts in median fluorescence intensity (MFI)

Table 1. PRAME expression, Pr20 binding, and surface HLA-A2 expression on cancer cell lines

Cell line	Tumor origin	*PRAME* mRNA	Pr20 binding	Surface HLA-A2
BV173	B-ALL	+	+	+++
AML14	AML	++	+++	+++
SET2	AML	+	++	++
THP-1	AML	++	+	+
U266	Myeloma	++	+	+++
MAC1	T lymphoma	++	+++	+++
MAC2A	T lymphoma	++	+++	+++
SK-Mel5	Melanoma	+++	+	+++
SK-Mel30	Melanoma	+	–	+
SK-Mel2	Melanoma	+++	–	+++
SK-Mel37	Melanoma	+++	–	++
UACC257	Melanoma	+++	–	++
UACC62	Melanoma	+++	–	+
A375	Melanoma	++	–	+
SW480	Colon adenocarcinoma	+	–	++
B-JAB	Burkitt lymphoma	+	–	++
SUDHL1	Lymphoma	+	–	++
SUDHL4	B lymphoma	+	–	++
PC9	Non–small cell lung	+	–	+
NCI-H2228	Non–small cell lung	–	–	++
SKLY16	B lymphoma	–	–	++
MDA-MB231	Breast adenocarcinoma	–	–	++
HL60	AML	++	–	–

PRAME expression in a panel of cell lines was determined by qPCR, and expression was binned into the follow groups based on relative expression to the constitutive gene *TBP* as calculated by standard $2^{-\Delta Ct}$ method based on a standard 40-cycle qPCR: negative (–) = no amplification; low (+) = <0.01; medium (++) = <5; and high (+++) = >5. Surface HLA-A2 expression and Pr20 binding were determined by flow cytometry with the following bins determined by MFI relative to an isotype control. Pr20 binding was binned based on Pr20 MFI/isotype MFI: negative (–) = <2; low (+) = <5; medium (++) = <10; and high (+++) = >10. Surface HLA-A2 was binned based on HLA-A2 MFI/isotype MFI: negative (–) = <2; low (+) = <10; medium (++) = <50; and high (+++) = >50.

were detected compared with an isotype control in 3 samples, and there was no relationship to *PRAME* mRNA levels as measured by qPCR. Several primary AMLs that had high expression of *PRAME* by mRNA did not bind Pr20, suggesting that mRNA expression alone was insufficient for Pr20 binding and that additional regulatory mechanisms are required for cell-surface presentation of the ALY peptide. While mRNA expression may not always equate to sufficient protein expression, which is required for generation of the ALY peptide, we pursued a detailed investigation of the ALY presentation process as described below.

Pr20M mediates Ab-dependent cellular cytotoxicity against PRAME⁺ leukemia. Therapeutic mAbs can mediate cytotoxicity by various mechanisms, including direct cytotoxicity and Ab-dependent cellular cytotoxicity (ADCC), but low expression of peptide/HLA-I epitopes can reduce activity of the TCRm. To study whether Pr20 could be cytotoxic against leukemia, we engineered an afucosylated Fc form of the Ab (designated Pr20M) that provides enhanced effector recruitment properties via increased FcR affin-

ity. Such Fc sugar modifications are well established as enhancing mAb-mediated ADCC (32–35). Pr20M's ability to mediate ADCC in vitro was assessed on PRAME⁺ leukemia in the presence of healthy human donor PBMC effectors. We demonstrated that Pr20M could direct ADCC against PRAME⁺HLA-A2⁺ leukemia AML14, SET2, BV173, and lymphoma line MAC2A in a dose-dependent manner in vitro (Figure 2A). Pr20M did not mediate substantial ADCC against the PRAME⁺HLA-A2⁻ HL60 leukemia or the PRAME⁻HLA-A2⁺ lymphoma SKLY16, confirming Pr20M specificity. To determine whether Pr20M would direct cytotoxicity against healthy cells, we performed overnight autologous killing assays on HLA-A2⁺ PBMCs in the presence of Pr20M. Pr20M did not mediate depletion of T cells (CD3⁺), B cells (CD19⁺), myeloid cells (CD33⁺), or monocytes (CD14⁺) in healthy HLA-A2⁺ PBMCs in vitro (Figure 2B), indicating the lack of toxicity to the major normal hematopoietic lineages. As a positive control in the same assay, PRAME⁺HLA-A2⁺ lymphoma cells (MAC2A) were depleted by approximately 50%.

TCRm Abs have been observed as mediating direct cytotoxicity using effector-independent mechanisms, such as triggering caspase-mediated apoptosis (36). To investigate whether Pr20M mediated direct cytotoxicity, we incubated Pr20M with PRAME⁺HLA-A2⁺ leukemia in vitro for 48 or 72 hours and assayed for metabolically viable cells. Pr20M did not substantially affect viability or cause growth inhibition in vitro (Supplemental Figure 2), suggesting that Pr20M does not mediate direct cytotoxicity and requires immune effector cells for redirected lysis.

Pr20M is therapeutically active against disseminated leukemia models in vivo. To determine the therapeutic utility of the afucosylated Pr20M TCRm, pharmacokinetics and biodistribution were examined in vivo. Pr20M exhibited a blood serum pharmacokinetic half-life of approximately 4.5 days in C57BL/6 mice, similar to other reported TCRm, demonstrating that Pr20M was stable in vivo (Supplemental Figure 3A). This serum half-life was similar to that of other reported TCRm (33). Although murine PRAME protein does not contain the ALY peptide, HLA-A2 transgenic mice can be used for potential off-target binding and toxicity studies, as the HLA-A2 can present potential crossreactive murine protein–derived epitopes that might be shared with the human proteome. Biodistribution studies in HLA-A2 transgenic mice showed that at 24 hours, there was no substantial Ab sink in any organ examined compared with isotype control Abs (Supplemental Figure 3B), suggesting no organ-specific or widely HLA-A2–presented murine peptide sequences were recognized by Pr20. While the mouse and human proteome are not identical, they are homologous. Taken together, our data suggest that Pr20 is relatively specific to the ALY sequence and that potential crossreactive sequences are not processed or presented in normal mouse tissues.

To determine whether Pr20M could be therapeutically active against leukemia models, B, T, and NK cell–deficient nonobese diabetic/severe combined immunodeficiency/IL-2 receptor gamma deficient (NSG) mice (37) were xenografted with HLA-A2⁺/PRAME⁺ human leukemias BV173 (ALL), SET2 (AML), and AML14 (AML), which were transduced to express GFP and luciferase. Mice were treated twice a week with 50 μg of Pr20M from day 6 or 7 until the experiment end point. Pr20M significantly reduced the growth of BV173, SET2, and AML14, as measured by bioluminescent imaging (BLI) (Figure 3, A–C) in vivo. In the BV173 model,
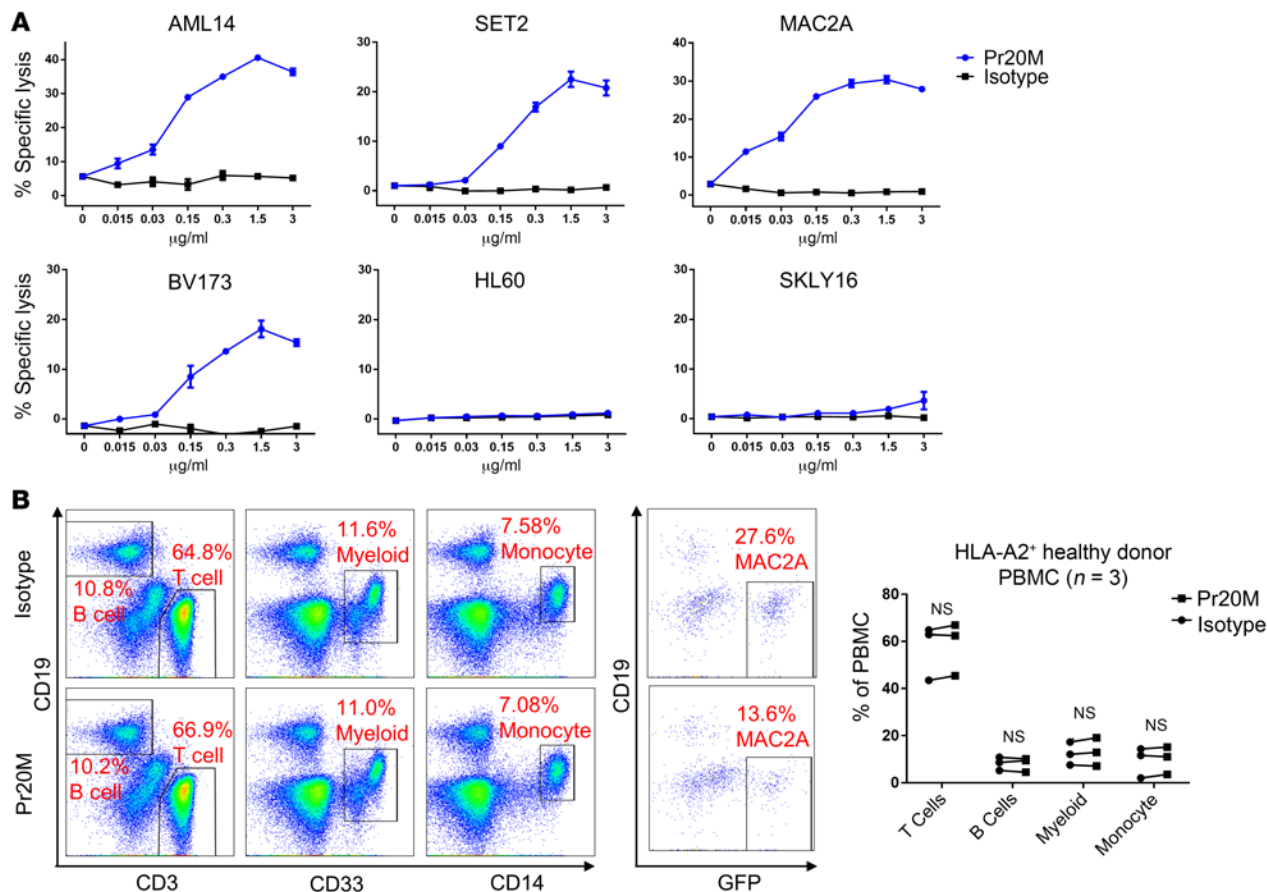
Figure 2. Pr20M mediates Ab-dependent cellular cytotoxicity in vitro on PRAME⁺HLA-A2⁺ leukemias and lymphoma. (**A**) ADCC assay was performed on hematopoietic cancers. ⁵¹Cr-labeled target leukemia or lymphoma cells were incubated with healthy donor PBMCs at an effector/target ratio of 50:1. Pr20M or an afucosylated isotype control Ab was added at the indicated concentration. Supernatant was collected after 6 hours, and scintillation counting was used to determine percentage of specific lysis. Data represent at least 3 experiments for each cell line except SKLY16 and MAC2A (done twice). (**B**) Healthy donor PBMCs were incubated overnight with 1 μg/ml of Pr20M or afucosylated isotype control. Flow cytometry was used to determine populations of B cells (CD19⁺CD3⁻), T cells (CD3⁺CD19⁻), monocytes (CD14⁺CD19⁻), and myeloid cells (CD33⁺CD19⁻). One representative analysis (n = 3) is shown, including a positive control to demonstrate that PBMCs in all assays were capable of depleting a PRAME⁺HLA-A2⁺ lymphoma (CD19⁻ and transduced with GFP). Data from HLA-A2⁺ healthy donor PBMCs (n = 3) performed independently are summarized and plotted. Data analyzed by paired Wilcoxon signed-rank test.

Pr20M-treated mice at day 13 had reduced leukemia burden compared with day 6 (Figure 3A). In the AML14 model, 3 out of 4 mice in the isotype-treated group succumbed to severe hind-leg paralysis by day 29, whereas none of the Pr20M-treated mice displayed such clinical signs. On day 29, recurrent AML14 leukemia was examined in the bone marrow. Bone marrow leukemia burden was significantly reduced in mice treated with Pr20M, as measured by flow cytometry (Figure 3D). No downmodulation of HLA-A2 or the Pr20 epitope was detected in AML14 cells harvested from Pr20M-treated mice compared with isotype-treated mice (Figure 3E). Target downregulation was therefore not a major mechanism of resistance to Pr20M in these models, confirming previously described observations with other TCRm therapies (38). Our data demonstrate that Pr20M has broad therapeutic activity against several human leukemias.

PRAME protein expression alone is not sufficient for Pr20 binding, but IFN-γ can enhance Pr20 binding in PRAME⁺ solid tumors and enhance ADCC. Interestingly, neither *PRAME* mRNA levels nor PRAME protein levels correlate with Pr20 cell-surface

binding. Several HLA-A2⁺ cancers that expressed high levels of PRAME, such as the melanoma cell lines SK-Mel5, UACC257, and A375, did not readily bind Pr20 (Table 1). Therefore, we hypothesized that PRAME and HLA-A2 expression alone are necessary but not sufficient to generate the ALY/HLA-A2 complex. Hematopoietic cells are well known to express an alternative form of the proteasome called the immunoproteasome (24), and indeed, most PRAME-positive leukemias bound Pr20. We hypothesized that the immunoproteasome is important for processing the ALY peptide. Although not highly expressed in most tissues, the immunoproteasome can be upregulated by proinflammatory cytokines such as IFN-γ and TNF-α (26).

PRAME⁺ melanoma cell lines SK-Mel5, UACC257, and A375 and a PRAME⁺ colon adenocarcinoma, SW480, were treated with IFN-γ for 72 hours to induce immunoproteasome expression. Upon IFN-γ treatment, these cell lines showed dramatically increased binding to Pr20 (Figure 4A). As IFN-γ can cause upregulation of HLA-I, it was possible that the increased Pr20 binding was partly driven by increased cell-surface HLA-A2.
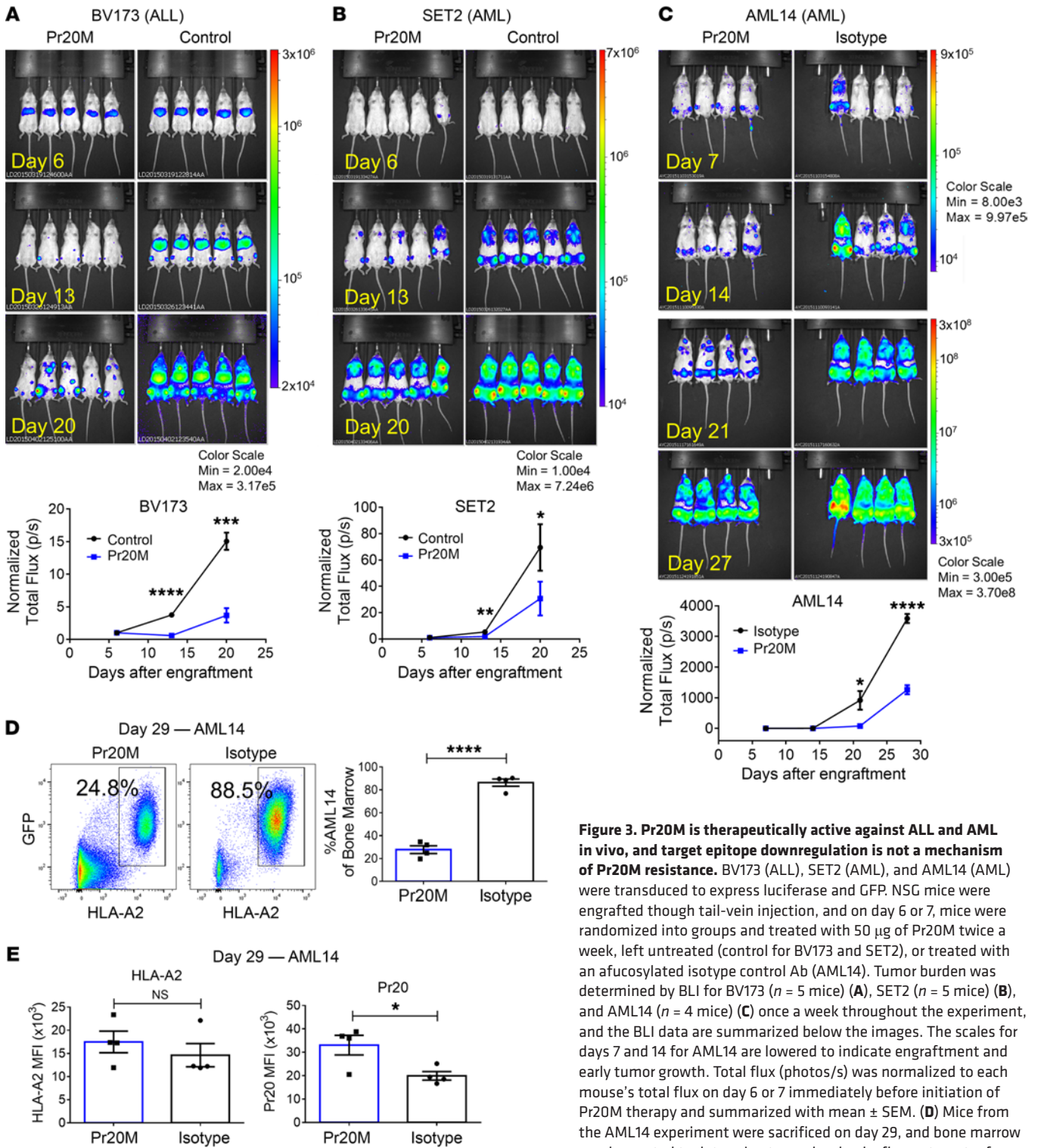
Figure 3. Pr20M is therapeutically active against ALL and AML in vivo, and target epitope downregulation is not a mechanism of Pr20M resistance. BV173 (ALL), SET2 (AML), and AML14 (AML) were transduced to express luciferase and GFP. NSG mice were engrafted though tail-vein injection, and on day 6 or 7, mice were randomized into groups and treated with 50 μg of Pr20M twice a week, left untreated (control for BV173 and SET2), or treated with an afucosylated isotype control Ab (AML14). Tumor burden was determined by BLI for BV173 (*n* = 5 mice) (**A**), SET2 (*n* = 5 mice) (**B**), and AML14 (*n* = 4 mice) (**C**) once a week throughout the experiment, and the BLI data are summarized below the images. The scales for days 7 and 14 for AML14 are lowered to indicate engraftment and early tumor growth. Total flux (photos/s) was normalized to each mouse's total flux on day 6 or 7 immediately before initiation of Pr20M therapy and summarized with mean ± SEM. (**D**) Mice from the AML14 experiment were sacrificed on day 29, and bone marrow was harvested to determine tumor burden by flow cytometry for GFP+HLA-A2+ AML14 cells. Representative plots (*n* = 4 mice per group) are shown, and data are summarized. (**E**) MFI of AML14 for HLA-A2 and Pr20 was determined by flow cytometry. Because Pr20M-treated mice presumably had Pr20M already bound on tumor cells, staining was performed by an additional Pr20 stain on all samples followed by a secondary PE-conjugated anti-human Ab (*n* = 4 mice per group). Experiments were performed once per model. Differences were evaluated using the unpaired *t* tests on indicated times and samples. AML14 BLI data are representative of 3 similar experiments, while SET2 and BV173 BLI data are from 1 experiment. *P < 0.05; **P < 0.01; ***P < 0.001; ****P < 0.0001.
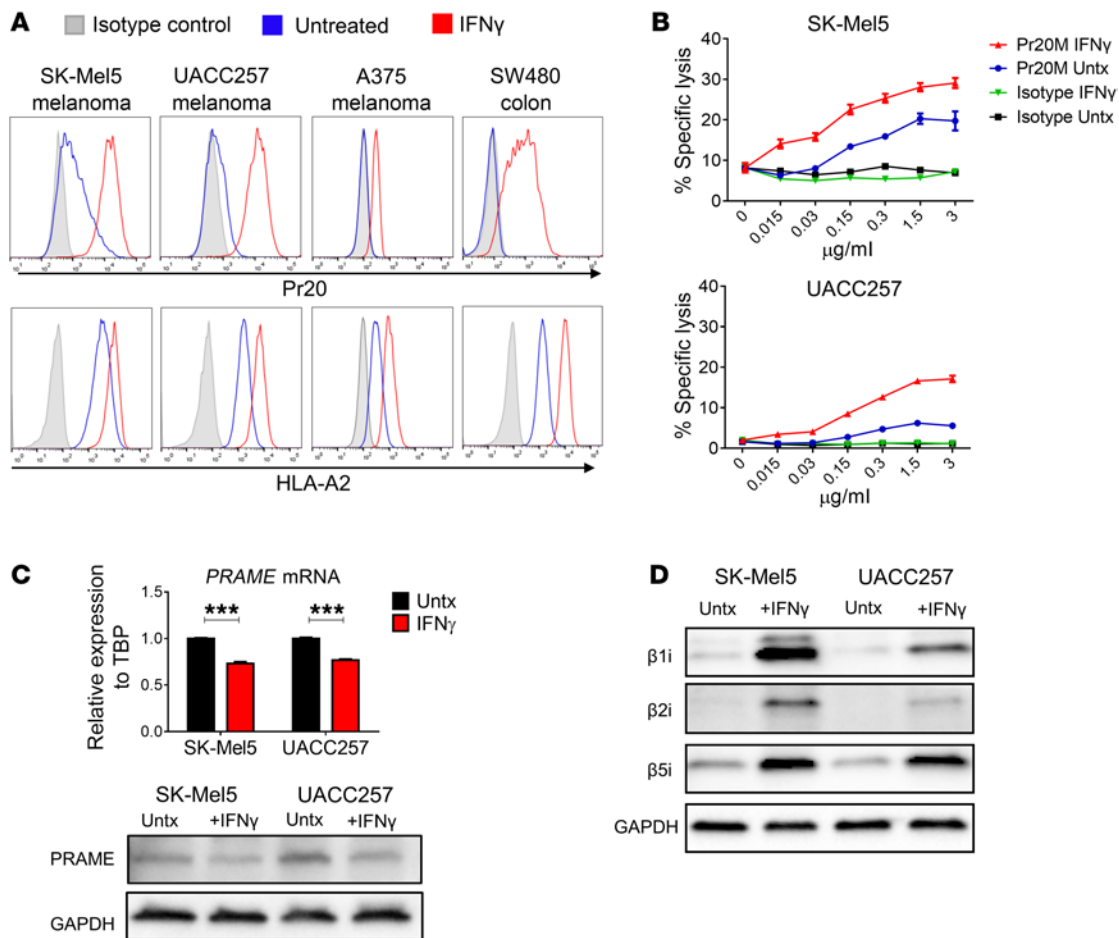
Figure 4. Melanomas and other solid tumors do not readily bind Pr20, but treatment with IFN-γ induces immunoproteasome expression and dramatically increases Pr20 binding. (**A**) HLA-A2⁺ melanomas and a colon adenocarcinoma that expressed *PRAME* by qPCR (Table 1) were either left untreated (blue) or treated with 10 ng/ml of IFN-γ for 72 hours (red) and stained with Pr20 compared with untreated cells stained with an isotype control Ab (gray). HLA-A2 staining was performed in parallel. Data represent 3 independent experiments. (**B**) Melanomas were pretreated with 10 ng/ml IFN-γ for 72 hours or left untreated before ⁵¹Cr-ADCC assay was used to determine specific lysis by Pr20M. Samples were assayed in 3 technical replicates, and data are representative of 3 experiments per cell line. (**C**) PRAME expression after 72 hours of IFN-γ treatment was also measured by qPCR and Western blot analysis. qPCR data were analyzed by unpaired *t* test and are representative of 3 experiments with 3 technical replicates per experiment where mean ± SEM are plotted. Western blot data are representative of 3 experiments. (**D**) The expression of each immunoproteasome subunit was also determined after IFN-γ treatment by Western blot analysis. Blots were derived from replicate samples run on parallel gels with the GAPDH loading control shown from the β2i blot. Data are representative of 3 experiments.

However, Pr20 binding increased far more (up to 10-fold) than HLA-A2 (2- to 6-fold) (Figure 4A), suggesting that increases in HLA-A2 were not the dominant cause of the increased Pr20 binding. Importantly, pretreatment of the tumor cells with IFN-γ led to enhanced Pr20M-mediated ADCC in vitro, indicating that upregulation of the target epitope might enhance therapeutic utility (Figure 4B). Increased Pr20 binding was not observed in several samples of HLA-A2⁺ healthy donor PBMC populations after IFN-γ treatment (Supplemental Figure 4). PRAME mRNA and protein expression did not increase after IFN-γ treatment and, indeed, decreased slightly (Figure 4C), suggesting that IFN-γ–mediated regulation of PRAME protein expression was not the cause of increased ALY peptide presentation. Protein expression of the immunoproteasome subunits β1i, β2i, and β5i increased after IFN-γ treatment (Figure 4D), possibly leading to enhanced generation of the ALY peptide.

The immunoproteasome catalytic subunit β5i is important for IFN-γ–mediated regulation of Pr20 binding. We hypothesized that IFN-γ could enhance generation of the ALY peptide by altering the proteasome components. To determine whether increased Pr20 binding was due to immunoproteasome upregulation, we generated CRISPR knockouts of each immunoproteasome subunit in the SK-Mel5 melanoma. After knockout by Cas9, β1i, β2i, and β5i were not measurable by Western blot analysis compared with a vector control (Figure 5A). The immunoproteasome subunit knockouts were treated with IFN-γ for 72 hours, and Pr20 binding was assessed by flow cytometry (Figure 5B). β5i knockout led to substantially less Pr20 binding, demonstrating that β5i plays an important role in IFN-γ–mediated processing of the ALY peptide epitope. CRISPR knockout of β5i yielded the same effect in UACC257, another PRAME⁺HLA-A2⁺ melanoma (Figure 5B), and SW480, an PRAME⁺HLA-A2⁺ colon adenocarcinoma (Supplemen-
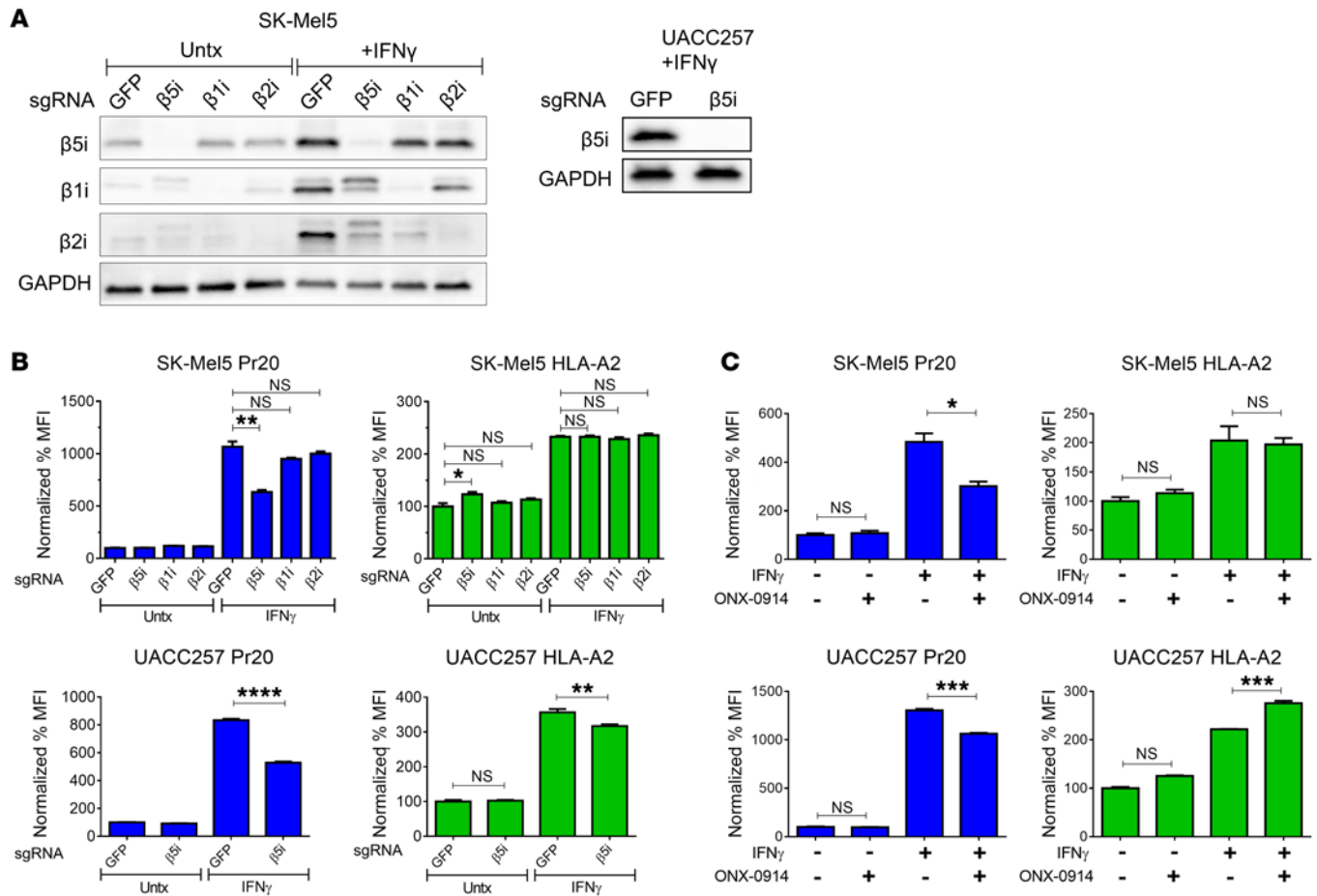
Figure 5. Immunoproteasome catalytic subunit β5i is important for IFN-γ–mediated Pr20 binding in melanomas and other solid tumors. β1i, β2i, and β5i were knocked out in the SK-Mel5 melanoma line using a CRISPR approach. A CRISPR construct against GFP was used as a vector control. (**A**, left panel) Cells were treated with 10 ng/ml IFN-γ for 72 hours, and Western blot analysis was used to demonstrate successful knockouts. Blots were derived from replicate samples run on parallel gels with the GAPDH loading control shown from the β2i blot. (**B**) Flow cytometry was used to determine Pr20 binding and surface HLA-A2 on the indicated knockouts (sgRNA against β1i, β2i, and β5i) untreated or treated with IFN-γ for 72 hours. (**B**, top panels). Data are normalized to MFI of untreated GFP sgRNA CRISPR control. (**B**, lower panels) β5i CRISPR knockout experiments were performed in the same manner on the UACC257 melanoma line. Successful knockout was determined by Western blot (**A**, right panel), and Pr20 binding and surface HLA-A2 were determined by flow cytometry (**B**, lower panels). (**C**) SK-Mel5 and UACC257 cells were left untreated or treated with 10 ng/ml IFN-γ for 72 hours in the presence or absence of 200 nM of the β5i inhibitor ONX-0914. Flow cytometry was used to determine MFI relative to untreated cells. All data are representative of 3 experiments with 3 technical replicates per experiment and mean ± SEM plotted. Statistical significance was determined by unpaired *t* test compared with control. *$P < 0.05$; **$P < 0.01$; ***$P < 0.001$; ****$P < 0.0001$.

tal Figure 5). Surface HLA-A2 expression was not affected by β5i knockout in the SK-Mel5 model and only minimally decreased in the UACC257 model (Figure 5B). ONX-0914, a selective inhibitor of β5i, was used to provide orthogonal validation that the immunoproteasome is important for generation of ALY/HLA-A2. SK-Mel5 and UACC257 were treated with IFN-γ for 72 hours with or without the presence of ONX-0914. ONX-0914 was used at 200 nM, a concentration reported to have potent biochemical inhibition of β5i, but minimal inhibition of other proteasome catalytic subunits (25). As expected, cells treated with ONX-0914 had reduced Pr20 binding compared with cells treated with IFN-γ alone (Figure 5C). Taken together, our data suggest the shift from the constitutive proteasome to the immunoproteasome is an important mechanism for increased epitope presentation and Pr20 binding. Furthermore, SK-Mel5 cells treated with bortezomib alone, a potent inhibitor of the constitutive proteasome β5 subunit and, to a lesser

extent, the β1 subunit (39), did not substantially alter binding to Pr20 at doses that were not cytotoxic. We also explored the use of demethylating agents in an attempt to increase the level of PRAME protein expression and thereby possibly peptide epitope on the surface. We observed only modest increases in Pr20 binding after decitabine treatment (Supplemental Figure 6).

The constitutive proteasome mediates internal destructive cleavage of the ALY peptide. Proteasomal degradation can regulate the generation of a specific HLA-I–associated peptide through enhancing the required N- or C-terminal cleavages or through reducing destructive internal cleavages. Several tumor-associated antigens exhibit restriction to the immunoproteasome because the peptide is largely destroyed by the constitutive proteasome and thus intact peptide cannot be presented (28, 40). To elucidate the differing proteolytic mechanisms between the constitutive and immunoproteasome involved in generating increased ALY peptide epitope on the sur-
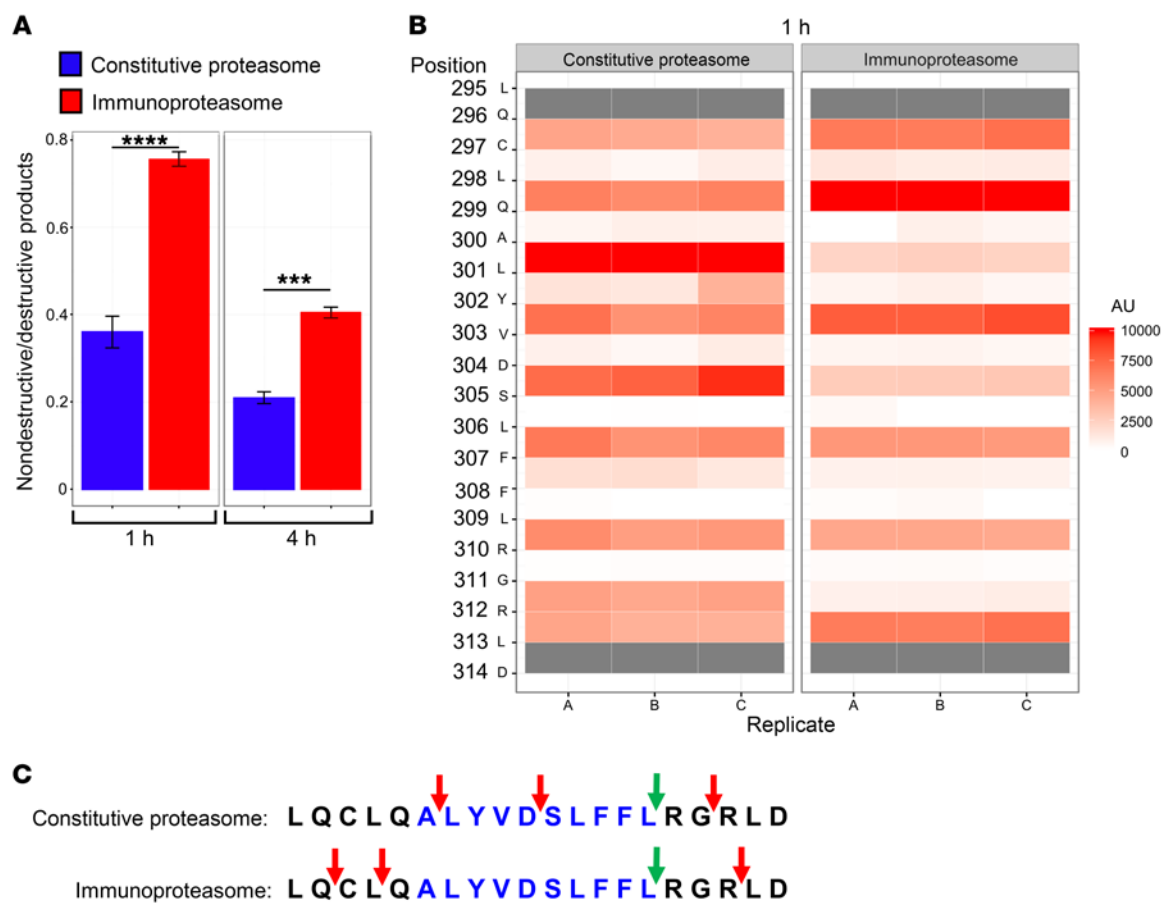
Figure 6. The immunoproteasome catalyzes increased nondestructive cleavages on an ALY-precursor peptide. A 20-mer ALY-elongated precursor peptide was incubated with purified constitutive proteasome or immunoproteasome for the indicated times. (**A**) All detectable fragments and their respective ion intensities were assigned to be nondestructive or destructive depending on whether the N- or C-terminal cleavages required to generate that fragment would have resulted in destruction of the ALY 10-mer. Ratios of ion intensity sums for nondestructive/destructive products are plotted. (**B**) Major cleavage sites along the precursor peptide after 1 hour were mapped by summing the ion intensities of each fragment resulting from a cleavage after the specific residue. Heat map with arbitrary units corresponding to ion intensities is shown, with 3 replicates illustrated in 3 bars for each proteasome preparation. Only fragments identified as at least 2 residues or more could be mapped, and thus cleavages before Q296 or after L313 were not accounted for. (**C**) Major differences in cleavage specificity between constitutive and immunoproteasome are schematized and mapped by red arrows. The green arrows denote the canonical proteasomal cleavage to generate the C-terminal end of the ALY 10-mer. Data are from 3 technical replicates per experimental condition with mean ± SEM plotted. Groups compared using multiple t tests. ***$P < 0.001$; ****$P < 0.0001$.

face, an elongated 20-mer ALY-precursor peptide was synthesized with 5 residues extending from each terminus (PRAME[295–314]). The ALY-precursor peptide was incubated with either purified constitutive proteasome or immunoproteasome in vitro, and digest fragments were analyzed by mass spectrometry. The major detectable fragments were then mapped to specific cleavage sites. Of the detected major digest fragments, the immunoproteasome had increased ratio of nondestructive/destructive cleavages in the ALY sequence (Figure 6A), while the immunoproteasome maintained the intact ALY 10-mer. In addition, the immunoproteasome catalyzed a major cleavage site after Q296 and L298 (LQ/CLQ**ALYVDSLFFL**RGRLD and LQCL/Q**ALYVDSLFFL**RGRLD, where bold letters indicate the ALY 10-mer) 1 and 3 residues N-terminal to the ALY 10-mer (Figure 6B). Such cleavage may prime the peptide for amino-peptidase trimming. In contrast, the constitutive proteasome mediated a major destructive cleavage site after A300 (LQCLQ**A**/**LYVDSLFFL**RGRLD) and after V303 (LQCLQ**ALYV**/**DSLFFL**RGRLD). Our analysis demonstrates that the relative

cleavage after the C-terminal L309 (LQCLQ**ALYVDSLFFL**/R-GRLD) was comparable between constitutive and immunoproteasome, suggesting that C-terminal cleavage of the ALY peptide was not a major mechanism of immunoproteasome restriction (Figure 6B). An N-terminal cleavage after the Q299 (LQCLQ/**ALYVD-SLFFL**RGRLD) was not a major cleavage site for either proteasome form. The major differences in cleavage specificities between the constitutive and immunoproteasome on the precursor peptide are schematized (Figure 6C). Taken together, the biochemical data show that the immunoproteasome enhances generation of the ALY 10-mer peptide through decreased internal destructive cleavage and increased N-terminal upstream cleavage, relative to the constitutive proteasome.

Discussion

Immunotherapy has demonstrated potent clinical utility for several cancers. However, successful therapy would be improved by use of targets that are cancer selective to minimize toxicity to

essential healthy tissue. Although highly selective onco-fetal or cancer-testis tumor-associated antigens have been described, most are intracellular proteins that cannot be targeted by small molecule inhibitors or by using Abs directed at cell-surface targets. Furthermore, most of these tumor antigens, such as PRAME, have context-dependent function and are not necessarily oncogenic. Thus, functional inhibition may not offer therapeutic benefit. Several groups have studied TCR-transgenic T cells specific against intracellular tumor-associated antigens, but this strategy has been limited due to challenges of large-sale manufacturing and safety concerns of the transgenic TCR recombining with the native TCR, generating unknown specificity and possible autoimmune reactivity (41). Recently described "ImmTAC" molecules use a TCR-based recognition domain offering similar reactivity to TCRm Abs, but they are typically 100-fold lower affinity (42). Instead, TCRm Abs such as Pr20 can target these "undruggable" proteins with high affinity for redirected immune-mediated cytolysis.

Pr20 specificity analyses were consistent with binding to the ALY peptide primarily on the C-terminal half amino acids at positions 5–9. However, because minimal contact residues were predicted in the N terminus, we cannot exclude the possibility of crossreactive peptide/HLA-A2 epitopes in the exome that share high C-terminal homology to ALY. Whether other theoretical peptide epitopes in the exome are expressed and processed appropriately in normal tissues is difficult to explore. The data shown here suggest that if potential crossreactive peptides in the human exome are expressed, properly processed, and sufficiently presented, they are infrequent. Peptides have specific processing requirements, including not only proteasomal degradation, but also aminopeptidase and oligopeptidase processing (43), which likely limit generation of crossreactive epitopes. In addition, potential crossreactive peptides may lack high affinity to HLA-A2 and thus will not form stable peptide/HLA-A2 complexes at the cell surface. Pr20 did not bind PRAME⁻HLA-A2⁺ cells and did not bind more than a dozen other HLA-A2⁺ tumor lines, suggesting there were no broadly presented crossreactive peptides. In addition, Pr20 did not bind to or accumulate in any major organ in HLA-A2 transgenic mice, nor bind to normal human blood cell populations in healthy HLA-A2⁺ donors. Taken together, the data suggest that crossreactive epitopes presented on HLA-A2 are non-abundant. Importantly, such off-targets are not increased in normal cells after IFN-γ treatment.

The afucosylated Pr20M demonstrated therapeutic efficacy in vivo. Interestingly, at the experimental end point, Pr20 binding to AML14 extracted from Pr20M-treated mice was slightly higher than in AML14 extracted from isotype-treated mice. This is intriguing because, first, it shows that target downregulation is not a mechanism of tumor escape in this model, and second, it also suggests that cellular interactions during Pr20M therapy may increase epitope expression on target cells. This may be due to cytokines released by immune effectors during ADCC, as observed with other therapeutic Abs (44, 45). It is important to note that the NSG mouse xenograft poorly models the human effector populations and the cytokine milieu that would be produced in a patient. In addition, because HLA-I is well characterized as regulated by inflammatory cytokines and TCRm targets are presented in complex with HLA-I, it is possible that TCRm targets are regulated in

a "feed-forward" system where TCRm-mediated cytolysis leads to local cytokine release and increased target expression on neighboring tumor cells. Human IgG1 also has different affinities to mouse FcR and human FcR, and NSG mice lack functional NK cells and have defective macrophages and dendritic cells. Therefore, lack of and poorly functional effector cell populations in this model may limit efficacy of a TCRm that requires immune effectors for ADCC (38), which may in part explain the lack of tumor eradication and relapse within weeks. It is reasonable to hypothesize that TCRm therapy in an immunocompetent patient or model would demonstrate more potent therapy. To better understand the incomplete responses to the therapy in vivo, we tested whether combination of Pr20M Ab therapy with a second therapeutic TCRm Ab directed to an unrelated epitope also found on the target cells would increase therapeutic effects (Supplemental Figure 7). This would yield more than double the target epitope numbers on each cell and also rule out the issue of leukemia escape by downregulation or loss of the PRAME epitopes from the leukemia cells. No significant improvement in leukemia control was demonstrated in these experiments, further bolstering the argument that lack of effector cell function and effector cell numbers were the critical deficiencies, not lack of (or loss of) target PRAME epitopes on the leukemia.

Generating an immunocompetent syngeneic mouse model in which to test these agents is difficult because murine PRAME does not comprise the human ALY peptide, which would have to be introduced genetically along with the use of mice with transgenic human HLA-A2. It is also unknown whether the ALY peptide can be properly cleaved and processed by the murine antigen presentation machinery and presented on transgenic HLA-A2 molecules. Coinfusion of human immune cell populations into NSG mice may provide an alternative model for effector cells and cytokines in these mice, but also leads rapidly to graft-versus-host disease and graft-versus-leukemia activity, complicating the analysis, as seen in previous studies (15).

Binding studies demonstrated that Pr20 robustly bound to several PRAME⁺HLA-A2⁺ leukemias and lymphoma cell lines, but did not bind well to a small sample size (n = 9) of previously frozen PRAME⁺HLA-A2⁺ primary AML. This is consistent with the lack of binding to several PRAME⁺HLA-A2⁺ cancer cell lines. Our data demonstrate that PRAME and HLA-A2 expression alone is necessary, but insufficient for Pr20 binding. It is also important to note that the number of ALY peptide epitopes presented on HLA-A2 is highly limited (estimated at less than 0.1% of the HLA molecules on the surface based on Scatchard analyses) and may be below the detection limit of the flow cytometry assay with Pr20 in some cells. It is also possible that low epitope presentation is undetectable with our assays, yet sufficient to initiate redirected lysis; however, this could not be reliably studied with frozen primary AML samples.

Pr20 did not initially bind several PRAME⁺HLA-A2⁺ melanomas and other solid tumors despite high levels of PRAME expression, but Pr20 binding dramatically increased upon treatment with IFN-γ, which was partially mediated by increases in immunoproteasome β5i expression. β5i is well characterized as having chymotrypsin-like enzymatic activity, cleaving after hydrophobic amino acids (23). However, the specificity is complex and not fully understood. For instance, β5i cleavage can be inhibited by

the presence of an additional hydrophobic residue directly C-terminal of a site as demonstrated in vitro using the enolase-1 protein as a model substrate (46). IFN-γ decreased PRAME protein expression, which may be caused by decreased mRNA expression but may also be due to differing kinetics of the immunoproteasome. Using a biochemical digestion assay in vitro, we demonstrated that the immunoproteasome cleaves and yields a presentable ALY-precursor peptide more efficiently then the constitutive proteasome. ALY peptide precursors generated through proteasomal digestion in vitro have been described (18); however, direct comparison between constitutive proteasome and immunoproteasome on digestion of the ALY peptide has not been studied. The constitutive proteasome catalyzed a major destructive cleavage site after the first A300 of ALY (LQCLQ**A**/**LYVDSLFFL**R-GRLD), whereas the immunoproteasome did not, possibly due to inhibition by the adjacent hydrophobic leucine. In addition, the immunoproteasome better catalyzed cleavages slightly N-terminal to the ALY peptide. Minor N-terminal elongated intermediate peptide may prime the peptide for aminopeptidase trimming into the ALY 10-mer; however, this was not studied. The knowledge of target presentation has broad implications when designing peptide vaccines, TCR, and TCRm Abs for determining which tumors may respond best to these therapies. In addition, checkpoint blockade therapy, which has demonstrated effective clinical utility, relies on tumor-antigen presentation and CTL recognition to direct tumor cell lysis. Therefore, understanding the biochemical mechanisms of immunogenic peptide generation and presentation is critical for designing checkpoint blockade strategies and determining ideal tumor targets. Our data suggest that tumors expressing the immunoproteasome such as leukemia and lymphomas would better respond to immunotherapies against ALY/HLA-A2 and that other cancer types may need pharmacologic upregulation of the immunoproteasome in conjunction to make the immunotherapy effective.

Pr20 binding requires peptide presentation in the context of HLA-A2, and thus strategies to enhance HLA-A2 expression may also augment Pr20M-mediated therapy. It will be important to discover pharmacological modulators of HLA-I that can be used for combination therapy with TCRm Abs or other HLA-I–based immunotherapies. For example, recent reports demonstrate that inhibition of MEK can increase cell-surface HLA-I, which may enhance TCRm Ab therapy (47). Additionally, several pharmacological agents that target histone-modifying enzymes, such as methyltransferase inhibitors and histone deacetylase inhibitors, can induce expression of tumor-associated antigens, including PRAME, and lead to enhanced cytolysis by effector T cells (48–50). It would be important to understand whether these agents could enhance antigen expression and synergize with TCRm therapy. However, these epigenetic drugs can also have context-dependent effects on immune cell function and therefore must be evaluated carefully to ensure they do not also inhibit the effector cells required for TCRm-mediated cytotoxicity (49, 51).

Our data demonstrate the ability to target PRAME with a TCRm Ab. This approach enables us to target intracellular proteins that cannot be modulated with small molecule inhibitors. TCRm allow access to a new universe of Ab protein targets, far larger and more tumor specific than the currently available

cell-surface protein targets. They also bypass the patient-specific limitations of CTL-based therapies. Only a few TCRm have been studied in preclinical models as agents for cancer therapy (15, 29, 36, 52–55). Therefore, the present study on Pr20 adds additional proof-of-concept that TCRm can be potent and selective therapeutic agents. Finally, due to the well-characterized mAb format of TCRm, they can be readily engineered into alternative formats such as Fc-enhanced forms, as shown in this study, and BiTE (56, 57) forms, as done with a TCRm to WT1, or transduced as chimeric antigen constructs (CARs) in T cells (58, 59). These additional formats may be required for effective targeting of these ultra–low density targets. Radioimmunoconjugates (60) and Ab-drug conjugates may also be explored in the context of TCRm in an effort to enhance potency against cancer cells.

Methods

Peptides. All peptides were purchased and synthesized by and purchased from Genemed Synthesis Inc. The peptides were dissolved in dimethyl sulfoxide and frozen at −80°C. Peptide-pulsing experiments were performed by incubating TAP-deficient T2 cells overnight with 50 μg/ml of peptide with 20 μg/ml β2M in either serum-free media or in the presence of 5% dialyzed FBS overnight. Control peptides used were established HLA-A2–binding peptides RHAMM-R3 (ILSLELMKL) and EW (QLQNPSYDK). Experimental peptides included the ALY peptide (ALYVDSLFFL) and the elongated 20-mer ALY-precursor peptide (LQCLQALYVDSLFFLRGRLD).

Cells. PBMCs from HLA-typed healthy donors were obtained by Ficoll density centrifugation. Cell lines were maintained at MSKCC and were originally obtained from ATCC and frozen as aliquots in liquid nitrogen. BV173 was provided by H. J. Stauss (University College London, London, United Kingdom). The following cell lines were gifts from the listed labs at MSKCC: AML14 was a gift from Ross Levine; SET2 was a gift from Richard J. O'Reilly; SK-Mel5 and SK-Mel37 were gifts from Jedd D. Wolchok; and SUDHL1 and SUDHL4 were gifts from Anas Younes. SKLY16, PC9, SK-Mel30, and SK-Mel2 were from cell line banks at MSKCC. THP1, U266, A375, SW480, BJAB, NCI-H2228, MDA-MB231, T2, and HL60 were obtained from ATCC. UACC257 and UACC62 were obtained from the National Cancer Institute. MAC1 and MAC2A were gifts from Mads H. Andersen (University of Copenhagen, Copenhagen, Denmark). Cell lines of unknown HLA were HLA typed by the Department of Cellular Immunology at MSK-CC. All cell lines were cultured in RPMI 1640 supplemented with 10% FCS, 1% penicillin, 1% streptomycin, 2 mM L-glutamine, and 10 mM HEPES at 37°C and 5% CO_2.

ScFv clones specific for ALY peptide/HLA-A2 complexes. A human-derived scFv Ab phage display library (7 × 10^{10} clones) was used for the selection of mAb clones. Methods for selection and characterization of the scFv as well as engineering of full-length Pr20 are described in Supplemental Methods.

Flow cytometry. For cell-surface staining, cells were blocked using FcR blocking reagent (Miltenyi Biotec, 130-059-901) at the manufacturer's recommended dilution for 15 minutes on ice, then incubated with appropriate fluorophore-conjugated mAbs for 30 minutes on ice and washed twice before resuspension in a viability dye (either DAPI or propidium iodide at 1 μg/ml). Abs used include anti–HLA-A2 clone BB7.2-APC (eBioscience, 17-9876-42), BB7.2-FITC (MBL, K0186-4), anti–CD3-PerCP clone 7D6 (Invitrogen, MHCD0331), anti–CD19-

PE-Cy7 clone 1D3 (eBioscience, 25-0193-81), anti-CD33-BV711 clone WM53 (BioLegend, 303423), and CD14-PE clone 61D3 (eBioscience, 12-0149-42). Pr20 or its human IgG1 isotype control (Eureka Therapeutics, ET901) was conjugated to APC using the lightning-link kit (Innova Bioscience, 705-0010), and staining was performed at 3 μg/ml, which was determined to be a saturating concentration. Flow cytometry data were collected on a LSRfortessa (BD) or an Accuri C6 (BD) and analyzed with FlowJo V10 software.

ADCC. Cancer cell lines used as ADCC target cells were incubated with 50 μCi of ^{51}Cr for 1 hour at 37°C and washed 3 times to remove free ^{51}Cr. Indicated concentrations of Pr20M or matched isotype control hIgG1 (afucosylated Eureka Therapeutics ET901) were incubated with target cells and fresh PBMCs at effector/target ratios of 50:1 for 6 hours at 37°C. The assay was performed in 96-well format with 5,000 target cells per well and 250,000 PBMCs. The supernatant was harvested, and the cytotoxicity was measured by scintillation counting. For flow-based ADCC assays, PBMC and GFP$^+$ tumor target cells were incubated at effector/target ratios of 30:1 overnight with 1 μg/ml of Pr20M and flow cytometry was used to determine depletion of GFP$^+$ tumor percentage. PBMCs were also incubated alone with 1 μg/ml Pr20M to measure potential autologous toxicity to PBMC populations.

Western blot and qPCR analysis. Total cell lysate was extracted using RIPA buffer and quantified using the DC protein assay (Bio-Rad). 15–30 μg of protein was loaded and run on 4%–12% SDS PAGE gels. After 1 hour block with 5% milk at room temperature, immunoblotting was performed using the following Abs: anti-20s β5i (Enzo Life Science, BML-PW8845-0025), anti-20s β2i (Enzo Life Science, BML-PW8350-0025), anti-20s β1i (Enzo Life Science, BML-PW8840-0025), and anti-PRAME (Sigma-Aldrich, HPA045153). Abs were probed at the manufacturer's s recommended dilution overnight at 4°C before a secondary Ab conjugated to HRP was used for imaging. Replicate samples were probed using the indicated Abs when noted, or blots were stripped with Restore Western Blot Stripping Buffer (Thermo Fisher Scientific, 21063), reblocked with 5% milk, and reprobed with an anti–GAPDH-HRP direct conjugated Ab (Cell Signaling Technology, 3683) as a loading control. qPCR was performed using the TaqMan Real-Time PCR system. RNA was extracted using QIAGEN RNeasy, and 1 μg of RNA was reverse transcribed into cDNA using qScript cDNA SuperMix (Quanta Biosciences). TaqMan probes and primers were designed from "assay-on-demand" gene expression products (Applied Biosystems). Primers and probes were *PRAME* (assay ID number: Hs01022301_m1), and the endogenous reference gene control was TATA-box binding protein (TBP) (assay ID number: HS99999910). The results are presented as relative differences in expression versus the endogenous reference control gene (2$^{-\Delta Ct}$) or fold changes based on the differences of normalized Ct values compared with control samples, assuming optimal primer efficiency (2$^{-\Delta\Delta Ct}$). Samples that did not amplify after 40 cycles or amplified at an equal or later Ct value compared with a water sample were considered negative and are not plotted with a value.

CRISPR knockout studies. LentiCRISPRv2 (Addgene plasmid 52961) (61) was a gift from Feng Zhang (Broad Institute, Cambridge, Massachusetts, USA). Guide RNA sequences targeting the immunoproteasome subunits were as follows: β2i (*PSMB10*): GTCCCTCAC-GCACGCAAGAC; β5i (PSMB8): GTGCAGCAGACTGTCAGTAC, β1i (*PSMB9*): GGTGCCTTGCAGGGATGCTG. Cells were transduced with LentiCRISPRv2, and transduced cells were selected using 1–4

μg/ml puromycin for 48 hours. Successful knockout was confirmed by Western blot analysis.

Animals. Eight- to ten-week-old NOD.Cg-*Prkdc^{scid}* IL2rg^{tm1Wjl}/SzJ mice (NSG) were purchased from The Jackson Laboratory or obtained from the MSKCC animal breeding facility. Female mice were used for the BV173 and SET2 models, while male mice were used for the AML14 model. C57BL/6 and B6.Cg-Tg(HLA-A/H2-D) Enge/J mice (HLA-A2 transgenic mice) (6 to 8 weeks old) for biodistribution experiments were also purchased from The Jackson Laboratory and bred at MSKCC.

Therapeutic trials of Pr20M. GFP/luciferase-transduced AML14 cells were passaged once in NSG mice, and bone marrow was harvested to generate a subculture line that engrafted more consistently in vivo. Using this AML14 subculture line, 3 million cells were injected intravenously into 2 groups of NSG mice. On day 7, tumor engraftment between the 2 groups was confirmed by luciferase imaging to have minimal intergroup variation. Groups were blindly assigned to either treatment group (Pr20M or Isotype-treated). 50 μg of Pr20M or an afucosylated isotype control human IgG1 (afucosylated Eureka Therapeutics, ET901) was injected intravenously twice weekly (every 3 or 4 days) starting on day 7 until the experiment end point on day 29. Tumor growth was assessed by weekly BLI, and bone marrow was harvested on day 29 for flow cytometric analysis. For BV173 and SET2 therapy experiments, 0.5 × 10^6 SET2 cells and 3 × 10^6 BV173 were engrafted into NSG mice through tail-vein injection. Mice were treated with 50 μg of Pr20M on days 6, 10, 13, and 17 after engraftment or left untreated (control), and tumor burden was assessed by BLI on the indicated days.

Pharmacokinetic and biodistribution studies. Pr20 Ab was labeled with ^{125}I (PerkinElmer) using the chloramine-T method. 100 μg of Ab was reacted with 1 mCi ^{125}I and 20 mg chloramine-T, quenched with 200 mg Na metabisulfite, then separated from free ^{125}I using a 10-DG column equilibrated with 2% bovine serum albumin in PBS. Specific activities of products were in the range of 4 to 8 mCi/mg. 2.5 μg of radiolabeled mAb was administered intravenously into each mouse through retroorbital injection, and blood and/or organs were collected at indicated time points, weighed, and measured on a γ counter.

In vitro proteasome digestion and liquid chromatography–mass spectrometry/mass spectrometry analysis. A 20-mer PRAME sequence peptide (LQCLQ<u>ALYVDSLFFL</u>RGRLD) termed the precursor peptide, encompassing the ALY epitope, and elongated by 5 residues on each end was synthesized by Genemed and ensured to be over 95% pure by HPLC. The precursor peptide was dissolved in DMSO and stored at −80°C. Purified constitutive proteasome and immunoproteasome were purchased from Boston Biochem (E-360 and E-370, respectively). 10 μg of precursor peptide was mixed with either 5 μg of constitutive or immunoproteasome in 100 μl of assay buffer per replicate. Assay buffer consisted of 2 nM MgAc$_2$, 1 mM DTT, and 20 mM HEPES/KOH at a pH of 7.8. The reaction was incubated at 37°C, and at each time point, a 20 μl aliquot was removed and quenched with 2 μl of 10% TFA in water. Samples were stored frozen at −80°C until mass spectrometry (MS) analysis. Each sample was analyzed separately by microcapillary liquid chromatography (LC) with electrospray ionization coupled with tandem MS. We used a NanoAcquity LC System (Waters) with a 100-μm inner diameter × 10-cm length C18 analytical column (1.7 μm BEH130; Waters) configured with a 180-μm × 2-cm trap column coupled to a Q-Exactive Plus Mass

Spectrometer (Thermo Fisher Scientific). A nanoelectrospray source (Proxeon, Thermo Scientific) set at 1800 V and a 25-micron (with 10-micron orifice) fused silica nanoelectrospray needle (New Objective) were used to complete the nanoelectrospray interface. For each time point, the sample was diluted 1:20 in HPLC grade water with 0.1% (v/v) formic acid and 1 μl was loaded onto the trap column and washed with 3× loop volume of buffer A (water with 0.1% [v/v] formic acid); the flow was reversed through the trap column and the peptides eluted with a 90-minute linear gradient from 1%–50% buffer B (acetonitrile with 0.1% [v/v] formic acid) at 300 nl/min. The QE Plus was operated in automatic, data-dependent MS/MS acquisition mode with 1 MS full scan (400–1800 m/z) at 70,000 mass resolution and up to 10 concurrent MS/MS scans for the 10 most intense peaks selected from each survey scan. Survey scans were acquired in profile mode, and MS/MS scans were acquired in centroid mode at 17,500 resolution, an isolation window of 1.5 amu, and normalized collision energy of 27. AGC was set to 1×10^6 for MS1 and 5×10^4 and 100 ms IT for MS2. Charge exclusion of unassigned and greater than 6 enabled with dynamic exclusion of 15 seconds. Degradation products were identified and quantified by in silico analysis of MS data. Briefly, all HPLC peaks were identified using the findpeaks method in the pracma R package. For each retention time during which a HPLC peak appeared, the ms1 spectra was analyzed to identify the series of peaks. Identified peak series were matched to a database of all possible precursor peptide degradation products. Total intensity of each degradation product was quantified by adding up the intensities of each production. If 2 degradation products yielded the same peak series (e.g., FFL and LFF), intensity was assigned to each product in proportion to the a2 and b2 product ions.

Statistics. Values reported represent mean ± SEM unless otherwise noted. P values were calculated with GraphPad Prism 6 (GraphPad Software Inc.) using the paired Wilcoxon signed-rank test where appropriate or Student's t test (unpaired, 2 tailed) with $P < 0.05$ considered significant. Binding affinity of Pr20 was determined on AML14 cells using Scatchard analysis after linear transformation of [bound] and [bound]/[free] Pr20. The 2-phase exponential decay model was used for analyzing Pr20M pharmacokinetics. Experiments were performed at least 3 times unless otherwise noted.

Study approval. All animal studies were approved by the Institutional Animal Care and Use Committee (IACUC) at Memorial Sloan Kettering Cancer Center (New York, NY) under protocol number 96-11-044. After informed consent on and approval by MSKCC Institutional Review Board (IRB) #95-054 (New York, NY), PBMCs from HLA-typed healthy donors were obtained by Ficoll density centrifugation. Frozen cells from AML patients were obtained under specific biospecimen banking protocols at MSKCC after informed consent and research authorization.

Author contributions

AYC, TD, and DAS designed experiments, interpreted the data, and wrote the manuscript. AYC and TD did biochemical characterization of Pr20 and immunological studies. TD designed experiments for initial clone selection and characterization of Pr20. RSG performed molecular biology experiments and MS analysis. CAJ, AS, TK, and VZ performed technical cell biology, immunology, and biochemistry. MC performed mAb radiolabeling and pharmacology experiments. LD and MDM performed animal therapy experiments. RCH performed MS experiments and analysis. CL performed phage display selection, generation of mAbs, and manufacturing of mAbs. DAS was the principle investigator.

Acknowledgments

Address correspondence to: David A. Scheinberg, 1275 York Avenue, Box 531, New York, New York 10065, USA. Phone: 646.888.2190; Email: scheinbd@mskcc.org.

1. Wadelin F, Fulton J, McEwan PA, Spriggs KA, Emsley J, Heery DM. Leucine-rich repeat protein PRAME: expression, potential functions and clinical implications for leukaemia. *Mol Cancer*. 2010;9:226.

2. Ikeda H, et al. Characterization of an antigen that is recognized on a melanoma showing partial HLA loss by CTL expressing an NK inhibitory receptor. *Immunity*. 1997;6(2):199–208.

3. Epping MT, Bernards R. A causal role for the human tumor antigen preferentially expressed antigen of melanoma in cancer. *Cancer Res*. 2006;6(22):10639–10642.

4. Oberthuer A, Hero B, Spitz R, Berthold F, Fischer M. The tumor-associated antigen PRAME is universally expressed in high-stage neuroblastoma and associated with poor outcome. *Clin Cancer Res*. 2004;10(13):4307–4313.

5. Greiner J, et al. mRNA expression of leukemia-associated antigens in patients with acute myeloid leukemia for the development of specific immunotherapies. *Int J Cancer*. 2004;108(5):704–711.

6. Ding K, Wang XM, Fu R, Ruan EB, Liu H, Shao ZH. PRAME gene expression in acute leukemia and its clinical significance. *Cancer Biol Med*. 2012;9(1):73–76.

7. Radich JP, et al. Gene expression changes associated with progression and response in chronic myeloid leukemia. *Proc Natl Acad Sci U S A*. 2006;103(8):2794–2799.

8. Doolan P, Clynes M, Kennedy S, Mehta JP, Crown J, O'Driscoll L. Prevalence and prognostic and predictive relevance of PRAME in breast cancer. *Breast Cancer Res Treat*. 2008;109(2):359–365.

9. Gerber JM, et al. Characterization of chronic myeloid leukemia stem cells. *Am J Hematol*. 2011;86(1):31–37.

10. Epping MT, Wang L, Edel MJ, Carlée L, Hernandez M, Bernards R. The human tumor antigen PRAME is a dominant repressor of retinoic acid receptor signaling. *Cell*. 2005;122(6):835–847.

11. Tajeddine N, Gala JL, Louis M, Van Schoor M, Tombal B, Gailly P. Tumor-associated antigen preferentially expressed antigen of melanoma (PRAME) induces caspase-independent cell death in vitro and reduces tumorigenicity in vivo. *Cancer Res*. 2005;65(16):7348–7355.

12. Wadelin FR, et al. PRAME is a golgi-targeted protein that associates with the Elongin BC complex and is upregulated by interferon-gamma and bacterial PAMPs. *PLoS One*. 2013;8(2):e58052.

13. Rezvani K, et al. Ex vivo characterization of polyclonal memory CD8+ T-cell responses to

PRAME-specific peptides in patients with acute lymphoblastic leukemia and acute and chronic myeloid leukemia. *Blood*. 2009;113(10):2245–2255.

14. Weber G, et al. Generation of tumor antigen-specific T cell lines from pediatric patients with acute lymphoblastic leukemia-implications for immunotherapy. *Clin Cancer Res*. 2013;19(18):5079–5091.

15. Dao T, et al. Targeting the intracellular WT1 oncogene product with a therapeutic human antibody. *Sci Transl Med*. 2013;5(176):176ra33.

16. Quintarelli C, et al. Cytotoxic T lymphocytes directed to the preferentially expressed antigen of melanoma (PRAME) target chronic myeloid leukemia. *Blood*. 2008;112(5):1876–1885.

17. Griffioen M, et al. Detection and functional analysis of CD8+ T cells specific for PRAME: a target for T-cell therapy. *Clin Cancer Res*. 2006;12(10):3130–3136.

18. Kessler JH, et al. Efficient identification of novel HLA-A(*)0201-presented cytotoxic T lymphocyte epitopes in the widely expressed tumor antigen PRAME by proteasome-mediated digestion analysis. *J Exp Med*. 2001;193(1):73–88.

19. Weber JS, et al. A phase 1 study of a vaccine targeting preferentially expressed antigen in melanoma and prostate-specific membrane antigen in patients with advanced solid tumors. *J Immunother*. 2011;34(7):556–567.

20. Gutzmer R, et al. Safety and immunogenicity of the PRAME cancer immunotherapeutic in metastatic melanoma: results of a phase I dose escalation study. *ESMO Open*. 2016;1(4):e000068.

21. Sakamoto S, Noguchi M, Yamada A, Itoh K, Sasada T. Prospect and progress of personalized peptide vaccinations for advanced cancers. *Expert Opin Biol Ther*. 2016;16(5):689–698.

22. Bassani-Sternberg M, Pletscher-Frankild S, Jensen LJ, Mann M. Mass spectrometry of human leukocyte antigen class I peptidomes reveals strong effects of protein abundance and turnover on antigen presentation. *Mol Cell Proteomics*. 2015;14(3):658–673.

23. Ferrington DA, Gregerson DS. Immunoproteasomes: structure, function, and antigen presentation. *Prog Mol Biol Transl Sci*. 2012;109:75–112.

24. Kincaid EZ, et al. Mice completely lacking immunoproteasomes show major changes in antigen presentation. *Nat Immunol*. 2011;13(2):129–135.

25. Muchamuel T, et al. A selective inhibitor of the immunoproteasome subunit LMP7 blocks cytokine production and attenuates progression of experimental arthritis. *Nat Med*. 2009;15(7):781–787.

26. Hallermalm K, et al. Tumor necrosis factor-alpha induces coordinated changes in major histocompatibility class I presentation pathway, resulting in increased stability of class I complexes at the cell surface. *Blood*. 2001;98(4):1108–1115.

27. Huber EM, et al. Immuno- and constitutive proteasome crystal structures reveal differences in substrate and inhibitor specificity. *Cell*. 2012;148(4):727–738.

28. Guillaume B, et al. Analysis of the processing of seven human tumor antigens by intermediate proteasomes. *J Immunol*. 2012;189(7):3538–3547.

29. Sergeeva A, et al. An anti-PR1/HLA-A2 T-cell receptor-like antibody mediates complement-dependent cytotoxicity against acute myeloid leukemia progenitor cells. *Blood*. 2011;117(16):4262–4272.

30. Bullinger L, et al. PRAME-induced inhibition of retinoic acid receptor signaling-mediated differentiation--a possible target for ATRA response in AML without t(15;17). *Clin Cancer Res*. 2013;19(9):2562–2571.

31. Ramsköld D, et al. Full-length mRNA-Seq from single-cell levels of RNA and individual circulating tumor cells. *Nat Biotechnol*. 2012;30(8):777–782.

32. Shinkawa T, et al. The absence of fucose but not the presence of galactose or bisecting N-acetylglucosamine of human IgG1 complex-type oligosaccharides shows the critical role of enhancing antibody-dependent cellular cytotoxicity. *J Biol Chem*. 2003;278(5):3466–3473.

33. Veomett N, et al. Therapeutic efficacy of an Fc-enhanced TCR-like antibody to the intracellular WT1 oncoprotein. *Clin Cancer Res*. 2014;20(15):4036–4046.

34. Umaña P, Jean-Mairet J, Moudry R, Amstutz H, Bailey JE. Engineered glycoforms of an anti-neuroblastoma IgG1 with optimized antibody-dependent cellular cytotoxic activity. *Nat Biotechnol*. 1999;17(2):176–180.

35. Chan AC, Carter PJ. Therapeutic antibodies for autoimmunity and inflammation. *Nat Rev Immunol*. 2010;10(5):301–316.

36. Verma B, et al. TCR mimic monoclonal antibodies induce apoptosis of tumor cells via immune effector-independent mechanisms. *J Immunol*. 2011;186(5):3265–3276.

37. Carreno BM, et al. Immunodeficient mouse strains display marked variability in growth of human melanoma lung metastases. *Clin Cancer Res*. 2009;15(10):3277–3286.

38. Dubrovsky L, et al. Mechanisms of leukemia resistance to antibody dependent cellular cytotoxicity. *Oncoimmunology*. 2016;5(9):e1211221.

39. Lü S, Wang J. The resistance mechanisms of proteasome inhibitor bortezomib. *Biomark Res*. 2013;1(1):13.

40. Ma W, et al. A MAGE-C2 antigenic peptide processed by the immunoproteasome is recognized by cytolytic T cells isolated from a melanoma patient after successful immunotherapy. *Int J Cancer*. 2011;129(10):2427–2434.

41. Stärck L, Popp K, Pircher H, Uckert W. Immunotherapy with TCR-redirected T cells: comparison of TCR-transduced and TCR-engineered hematopoietic stem cell-derived T cells. *J Immunol*. 2014;192(1):206–213.

42. Oates J, Hassan NJ, Jakobsen BK. ImmTACs for targeted cancer therapy: Why, what, how, and which. *Mol Immunol*. 2015;67(2 Pt A):67–74.

43. Kessler JH, et al. Antigen processing by nardilysin and thimet oligopeptidase generates cytotoxic T cell epitopes. *Nat Immunol*. 2011;12(1):45–53.

44. Agarwal A, Vieira CA, Book BK, Sidner RA, Fineberg NS, Pescovitz MD. Rituximab, anti-CD20, induces in vivo cytokine release but does not impair ex vivo T-cell responses. *Am J Transplant*. 2004;4(8):1357–1360.

45. Lee DW, et al. Current concepts in the diagnosis and management of cytokine release syndrome. *Blood*. 2014;124(2):188–195.

46. Toes RE, et al. Discrete cleavage motifs of constitutive and immunoproteasomes revealed by quantitative analysis of cleavage products. *J Exp Med*. 2001;194(1):1–12.

47. Brea EJ, et al. Kinase regulation of human MHC class i molecule expression on cancer cells. *Cancer Immunol Res*. 2016;4(11):936–947.

48. Schrump DS, et al. Phase I study of decitabine-mediated gene expression in patients with cancers involving the lungs, esophagus, or pleura. *Clin Cancer Res*. 2006;12(19):5777–5785.

49. Gang AO, et al. 5-Azacytidine treatment sensitizes tumor cells to T-cell mediated cytotoxicity and modulates NK cells in patients with myeloid malignancies. *Blood Cancer J*. 2014;4:e197.

50. Yan M, et al. Increased PRAME antigen-specific killing of malignant cell lines by low avidity CTL clones, following treatment with 5-Aza-2'-Deoxycytidine. *Cancer Immunol Immunother*. 2011;60(9):1243–1255.

51. Cao Q, et al. Inhibiting DNA methylation by 5-Aza-2'-deoxycytidine ameliorates atherosclerosis through suppressing macrophage inflammation. *Endocrinology*. 2014;155(12):4925–4938.

52. Cohen M, Reiter Y. T-cell receptor-like antibodies: targeting the intracellular proteome therapeutic potential and clinical applications. *Antibodies*. 2013;2(3):517–534.

53. Dubrovsky L, et al. T cell receptor mimic antibodies for cancer therapy. *Oncoimmunology*. 2016;5(1):e1049803.

54. Chang AY, et al. Opportunities and challenges for TCR mimic antibodies in cancer therapy. *Expert Opin Biol Ther*. 2016;16(8):979–987.

55. Dubrovsky L, et al. A TCR-mimic antibody to WT1 bypasses tyrosine kinase inhibitor resistance in human BCR-ABL+ leukemias. *Blood*. 2014;123(21):3296–3304.

56. Dao T, et al. Therapeutic bispecific T-cell engager antibody targeting the intracellular oncoprotein WT1. *Nat Biotechnol*. 2015;33(10):1079–1086.

57. Huehls AM, Coupet TA, Sentman CL. Bispecific T-cell engagers for cancer immunotherapy. *Immunol Cell Biol*. 2015;93(3):290–296.

58. Zhang G, et al. Anti-melanoma activity of T cells redirected with a TCR-like chimeric antigen receptor. *Sci Rep*. 2014;4:3571.

59. Rafiq S, et al. Optimized T-cell receptor-mimic (TCRm) chimeric antigen receptor T-cells directed towards the intracellular Wilms tumor 1 antigen [published online ahead of print January 3, 2017]. *Leukemia*. https://doi.org/10.1038/leu.2016.373.

60. McDevitt MR, et al. Tumor therapy with targeted atomic nanogenerators. *Science*. 2001;294(5546):1537–1540.

61. Sanjana NE, Shalem O, Zhang F. Improved vectors and genome-wide libraries for CRISPR screening. *Nat Methods*. 2014;11(8):783–784.